# Accepted Manuscript

Investigation of the Thermoelectric Response in Conducting Polymers Doped by Solid-State Diffusion

Keehoon Kang, Sam Schott, Deepak Venkateshvaran, Katharina Broch, Guillaume Schweicher, David Harkin, Cameron Jellett, Christian B. Nielsen, Iain Mcculloch, Henning Sirringhaus

Please cite this article as: K. Kang, S. Schott, D. Venkateshvaran, K. Broch, G. Schweicher, D. Harkin, C. Jellett, C.B. Nielsen, I. Mcculloch, H. Sirringhaus, Investigation of the Thermoelectric Response in Conducting Polymers Doped by Solid-State Diffusion, *Materials Today Physics*, https://doi.org/10.1016/j.mtphys.2019.02.004.

# Investigation of the Thermoelectric Response in Conducting Polymers Doped by Solid-State Diffusion

Keehoon Kang[1,2]*, Sam Schott[1], Deepak Venkateshvaran[1], Katharina Broch[1], Guillaume Schweicher[1], David Harkin[1], Cameron Jellett[3], Christian B. Nielsen[3,4], Iain Mcculloch[4,5], Henning Sirringhaus[1]*

1   Cavendish Laboratory, University of Cambridge, J. J. Thomson Avenue, Cambridge CB3 0HE, United Kingdom

2   Department of Physics and Astronomy, and Institute of Applied Physics, Seoul National University, Seoul 08826, Republic of Korea

3   Department of Chemistry and Centre for Plastic Electronics, Imperial College, London, SW7 2AZ, United Kingdom

4   Materials Research Institute and School of Biological and Chemical Sciences, Queen Mary University of London, London E1 4NS, United Kingdom

5   Physical Science and Engineering Division, King Abdullah University of Science and Technology (KAUST), Thuwal 23955-6900, Saudi Arabia

* Correspondence and requests for materials should be addressed to keehoon.kang@snu.ac.kr and hs220@cam.ac.uk

Thermoelectric effect is a physical phenomenon which intricately relates the thermal energy of charge carriers to their charge transport. Understanding the mechanism of this interaction in different systems lies at the heart of inventing novel materials which can revolutionize thermoelectric power generation technology. Despite a recent surge of interest in organic thermoelectric materials, the community has had difficulties in formulating the charge transport mechanism in the presence of a significant degree of disorder. Here, we analyze the thermoelectric properties of various conducting polymers doped by solid-state diffusion of dopant molecules based on a transport model with a power-law energy-dependence of transport function. A fine control of the degree of doping via post-doping annealing provides an accurate empirical evidence of a strong energy dependence of the carrier mobility in the conducting polymers. A superior thermoelectric power factor of conducting polymers doped by solid-state diffusion to that of other doping methods can be attributed to a resulting higher intrinsic mobility and higher free carrier concentration.

# 1  Introduction

Over the past 40 years, technologies developed for thermoelectric power generation has successfully met the power demands required for low-power applications in extraterrestrial space probes [1] and automotive thermoelectric generators used to harness waste heat from car engines which improves the fuel efficiency of the vehicle by up to around 5 % [2]. The main limitation for thermoelectric technology is a relatively low power conversion efficiency which can be quantified by the 'thermoelectric figure of merit', $zT = \frac{S^2\sigma}{\kappa}T$, where $S$ is the Seebeck coefficient, $\kappa$ is the thermal conductivity and $\sigma$ is the electrical conductivity of the material. Organic materials have a potential advantage due to their comparatively low thermal conductivity [3] and the community has put a concerted effort in achieving a high power-factor ($S^2\sigma$) to improve $zT$. Especially, creative molecular designs [4, 5, 6] and various treatment methods [7, 8, 9] have been developed to control the charge transport properties and degree of doping to further improve the power factor. A record power factor for organic materials was measured for a conducting polymer, poly(3,4-ethylenedioxythio-phene), doped with Tosylate (PEDOT:Tos [10]) reaching $460\mu Wm^{-1}K^{-2}$ which is around half of the power factor for a SnSe single-crystal.

However, there is still a lack of a clear understanding of charge transport mechanism in the organic systems which govern their thermoelectric properties. The Seebeck coefficient has been employed for elucidating the nature of charge transport in organic semiconductors (OSCs) and has been measured for both conjugated polymers [11, 12] and small-molecules [13, 14, 15] in field-effect transistor (FET) devices, at various charge densities in the accumulation layer induced by varying the gate voltage. The advantage of investigating thermoelectric properties with FET devices is that the field effect is less prone to dopant-induced-disorder which is generally present for chemically doped OSCs [16, 17]. However, the range of the charge density that can be induced in organic FETs is limited typically between $10^{18}$ and $10^{19}cm^{-3}$. Therefore the conductivity range in which the charge transport physics can be investigated is limited.

Venkateshvaran et al. [11] successfully explained the measured field-effect gated Seebeck coefficient of conjugated polymers with low energetic disorder over the range of charge

density $10^{18}$-$10^{19}$cm$^{-3}$ based on a narrow-band model which is applicable for polarons in a low disorder limit [18]. There is an open question as to whether such a model remains valid in a wider conductivity range where one might expect different charge transport regimes to appear. Recently, Glaudell et al. [16] showed an interesting phenomenological analysis that could describe the dependence of the Seebeck coefficient on conductivity of a wide range of polymers and dopant combinations that have been reported in literature, so far. An empirical relationship of $S = (k_B/e)(\sigma/\sigma_\alpha)^{-1/4}$, where $\sigma_\alpha$ is an unknown constant with the dimension of conductivity, gives a surprisingly good fit over a wide range of conductivities whereas conventional mobility edge and variable-range-hopping (VRH) model fail to explain the data over the wide range. However, the physical origin of such empirical model remains yet unclear. Kang et al. [19] recently proposed a model that accounts for an energy-dependent charge transport from which one can even derive the above empirical relationship as a limiting case for the model at a heavy-doping limit. The model relates $S$ and $\sigma$ to a transport function, $\sigma_E$, which is the contribution of states at energy $E$ towards the total conductivity. By predicting $\sigma_E$ to have a power-law dependence on $E$ with the power, $s$, above a transport edge below which the states do not contribute to the transport, they found that most of the reported data in literature fitted well with $s = 3$.

In this work, we investigated the thermoelectric properties of high-mobility conjugated polymers, poly(2,5-bis(3-hexadecylthiophen-2-yl)thieno[3,2-b]thiophene) (PBTTT),poly[2,6-(4,4-bis-alkyl-4H-cyclopenta-[2,1-b 3,4-b0 ]-dithiophene)-alt-4,7-(2,1,3-benzothiadiazole)] (cyclopentadithiophene-benzothiadiazole) (CDT-BTZ) and poly(3-hexyl- thiophene) (P3HT) doped by solid-state diffusion of 2,3,5,6-tetrafluoro-7,7,8,8-tetracyanoquinodimethane (F$_4$-TCNQ) [20]. We controlled the degree of doping by post-process annealing which allowed a systematic study of the Seebeck coefficient over a wide range of conductivities achieved by only a single combination of polymer and dopant. We have recently demonstrated that the solid-state diffusion doping is an efficient doping method which allows incorporation of the dopant with minimal structural and energetic disorder and perturbation of the conjugated polymer with high carrier mobilities. This results in favorable charge transport properties from which superior thermoelectric properties may be expected. In light of the recently proposed energy-dependent

charge transport model [19], we analyze the charge transport mechanism in these various conducting polymers to reveal crucial elements in determining thermoelectric power factors in these systems and potential limiting factors in conducting polymers in achieving high power factors.

## 2 Results & Discussion

Our previous work showed that solid-state diffusion doping with $F_4$-TCNQ achieved a high conductivity of 200 Scm$^{-1}$ in PBTTT when fully doped. The doping method was not only found to be efficient but also controllable via annealing the films after doping. The Fig. 1a shows a general concept of the method. A fully doped sample was consecutively annealed at different temperatures for 20 minutes on a hotplate in a controlled $N_2$ atmosphere to achieve de-doping. The de-doping cycle was limited to the temperature of 150 ℃ to minimize structural reorganization during annealing since it is the onset temperature for a thermotropic mesophase transition of PBTTT and side-chains melt completely above 160 ℃ [21]. The conductivity of these sequentially annealed films was measured by the 4-point probe method in a Hall-bar structure as we reported previously [20]. The range of conductivities that can be achieved with this de-doping method is significantly wider than the solution co-deposition technique (denoted as 'solution-doping' from here) employed by Cochran et al. [22]. The resulting conductivity drop via the annealing is confirmed to be a de-doping process rather than a degradation of the polymer from UV-Vis absorption data shown in Fig. 1b and c. The degree of bleaching of the neutral $\pi$-$\pi^*$ transition of PBTTT at 555 nm (2.2 eV) is decreasing (i.e. the neutral absorption recovers as the film gets de-doped). The charge-transfer doping creates polarons in PBTTT which show up optically as a broad polaron-induced absorption around 830 nm [23] which generally diminishes as we progress with de-doping. In addition to spectroscopic signatures of PBTTT, two peaks that correspond to $F_4$-TCNQ$^-$ at 767 and 869 nm on top of the P2 absorption [24] become less pronounced after annealing at 135 ℃. At the same time, the neutral absorption of $F_4$-TCNQ at 400 nm ($\approx$ 3.0eV) decreases throughout the de-doping process which indicates both $F_4$-TCNQ molecules which diffuse out from PBTTT and $F_4$-TCNQ molecules in the neutral layer (on top of the PBTTT film created during doping [20]) evaporate out of the film. Therefore, the

de-doping occurs via a reduction of the number of $F_4$-TCNQ available for charge-transfer in the PBTTT matrix.

There are other details of the doping/de-doping process that we can deduce from the spectra. The initial increase in the P2 absorption indicates that the degree of doping is higher for the 90 ℃ sample than the as-doped sample. This indicates that the solid-state diffusion of $F_4$-TCNQ molecules in PBTTT at room temperature is not sufficient to achieve a high degree of doping throughout the polymer film but that a thermal energy is required to re-distribute the dopant molecules within the film to achieve a homogeneous doping in the film. Therefore, the sample annealed at 80 ℃ (shown as the first data point in Fig. 1a) has a higher conductivity than the 'as-doped' sample. Furthermore, the neutral absorption of PBTTT does not recover to the full peak height of the pristine sample after the de-doping. The reduced absorption cross-section after a full cycle of de-doping could be due to either a finite degree of sample degradation or structural transformation or bleaching due to remaining charges. The de-doped sample could be re-doped as shown in Fig. 1c. The de-doping of re-doped sample shows qualitatively the same trend as in the first cycle (Fig. 1b) with a further reduced peak height for P2 absorption (near 830 nm) and a slightly smaller peak height for the neutral absorption of PBTTT (at 555 nm) after de-doping completely (150 ℃ annealing). The reason for this is not entirely clear and we have to investigate structural changes induced during the de-doping process which will be the topic of the next part.

As demonstrated in our previous work [20], the solid-state diffusion doping of PBTTT with $F_4$-TCNQ results in the dopant molecules intercalating in the alkyl side-chain regions, and therefore expanding the out-of-plane lamellar spacing. In this work, specular scans for XRD measurement were used to determine the out-of-plane lamellar spacing (see Fig. 2a) and grazing incidence X-ray diffraction (GID) measurement was performed with an area detector to measure in-plane diffraction peaks (see Fig. 2b) at different doping levels achieved with de-doping by annealing. As expected, the out-of-plane lamellar spacing measured by X-ray diffraction measurements (XRD) for a doped-film determined by $(h00)$ diffraction peaks along $q_z$ is 23.4Å (see Fig. 2c) which is bigger than that of a pristine sample (21.5Å) due to $F_4$-TCNQ

molecules intercalating in the side-chain region. The de-doping via annealing leads to contraction of the lamellar spacing with a significant reduction occurring after $135\,°C$. The annealing at $150\,°C$ reduces the d-spacing further to $21.7\text{Å}$ which is nearly identical to that of the pristine film. This indicates that $F_4$-TCNQ molecules diffuse out of the alkyl side-chain region to recover the lamellar stacking for a pristine PBTTT which is consistent with the UV-Vis measurement in Fig. 1b. The XRD measurements for a pristine PBTTT sample and after the de-doping step at $120\,°C$ were measured separately from the data shown in Fig. 2a and are shown in Fig. S4 in the Supplementary Information Section C.

The measured in-plane diffraction peaks along $q_{xy}$ (Fig. 2b) are at $q_{xy} = 1.41\text{Å}^{-1}$ which corresponds to (003) reflections [21, 25, 22] that represents periodicity along $c$-direction (i.e. the polymer backbone), and a peak around $q_{xy} = 1.70\text{Å}^{-1}$ which corresponds to $\pi$-$\pi$ stacking (periodicity along $b$-direction [25]). The peak at $q_{xy} = 1.41\text{Å}^{-1}$ is unaffected through doping and de-doping. The change in the $\pi$-$\pi$ stacking distance was found to be very small (below $0.15\text{Å}$) compared to the change in the $(h00)$ d-spacing of over $2\text{Å}$ and this could be a result of $F_4$-TCNQ molecules in the side-chain region causing steric perturbation to side-chains. This perturbation would cause tilting of the conjugated backbones to result in a closer $\pi$-$\pi$ stacking. The overall structural change in PBTTT doped by solid-state diffusion resembles that of poly(3-alkylthiophene) doped by iodine [26, 27] and electrochemical doping with various dopants [28]. Both the expansion of the out-of-plane lamellar spacing and the contraction of the $\pi$-$\pi$ stacking distance were associated with the incorporation of the dopant ions into a vacant space between alkyl side-chains [28], which is similar to our proposed structural model for PBTTT/ $F_4$-TCNQ. As the film gets de-doped, the $\pi$-spacing stays nearly the same ($3.47\text{Å}$ ) before the $120\,°C$ step from which the $\pi$-spacing gradually increases to $3.61\text{Å}$ after the $150\,°C$ step, very nearly recovering the $\pi$-spacing of $3.60\text{Å}$ for a pristine film (see Fig. 2d).

Both the out-of-plane and in-plane X-ray scattering peaks show no splitting or a significant broadening which indicates no phase-separation or creation with doping, e.g. pristine and doped phases co-existing in the film. Therefore, the doped PBTTT film maintains one-phase-structure without a complex phase behavior at every de-doping level. Interestingly,

the de-doping method was also found to preserve the structural order of PBTTT along the alkyl side-chain direction which can be indicated by similar crystallite sizes calculated with Williamson-Hall analysis of the measured $(h00)$ Bragg-peaks (see Supplementary Information Section D for more details).

In summary, the de-doping technique employed recovers the crystalline structure of the pristine PBTTT *without disrupting the structural order* along the side-chain direction via counteracting structural changes that occur upon doping due to the incorporation of F$_4$-TCNQ molecules. We are now in a position to qualitatively describe the de-doping mechanism. During the de-doping process, both the in-plane and out-of-plane structures remain fairly constant until the 120 °C annealing step. From the annealing step at 120 °C to 150 °C, there is a continuous transition of both the $\pi$ spacing and out-of-plane d-spacing. The gradual change represents a gradual reduction of the number of F$_4$-TCNQ molecules in the side-chain regions which diffuse out to the surrounding atmosphere, which is similar to the picture prosed by Li et al.. [29] The reason for a significantly more pronounced de-doping effect above 120 °C may be due to a significant thermal expansion of the lamellar spacing of PBTTT above 120 °C. Temperature-dependent XRD measurements of PBTTT [21] showed that the lamellar spacing expands by 0.5Å when heated from 90 °C to 120 °C which would allow more space for the F$_4$-TCNQ diffusion and accelerate de-doping. In addition, the diffusion is more rapid due to a higher thermal energy of F$_4$-TCNQ molecules. After the annealing, the film is cooled down to room temperature, and therefore the lattice contracts until the side-chains start to cause steric hinderance to the remaining F$_4$-TCNQ molecules in the region.

The de-doping method demonstrated above allows us to study the Seebeck coefficient versus conductivity over a wide range of conductivities for a single system of PBTTT doped by solid-state diffusion of F$_4$-TCNQ (denoted as 'PBTTT/ F$_4$-TCNQ' from here). The 4-point probe conductivity and the Seebeck coefficient could be simultaneously and accurately measured with on-chip micro-fabricated devices by employing a structure shown in Fig. 3a and three of these devices were measured in total (the measurement configuration is given in Supplementary Information Section A). The Seebeck coefficient and conductivity values of the three devices

agreed well with each other within the measurement error when fully doped. We could measure the change in the conductivity of the as-doped sample after each of the sequence of annealing steps (described in the Supplementary Information Section B).

The measured Seebeck coefficient at each de-doping level could be well described with a model proposed by Kang et al. [19] which assumes that the transport function has a power-law energy dependence with the power, $s$, above a transport edge, $E_t$ below which carriers are completely localized and do not contribute to the transport. One can express the conductivity, $\sigma$, and the Seebeck coefficient, $S$, of a system as a sum of contribution of states at each $E$ as [30]

$$\sigma = \int \sigma_E \left(-\frac{\partial f}{\partial E}\right) dE \tag{1}$$

$$S = \frac{k_B}{e} \int \frac{(E-E_F)}{k_B T} \frac{\sigma_E}{\sigma} \left(-\frac{\partial f}{\partial E}\right) dE, \tag{2}$$

where $f(E)$ is the Fermi-Dirac distribution function and $\sigma_E(E)$ is the transport function. The model by Kang et al. assumes $\sigma_E = \sigma_{E_0}(T) \times \left(\frac{E-E_t}{k_B T}\right)^s$ for $E > E_t$, where $\sigma_{E_0}$ is an effective transport coefficient which depends on temperature but not on energy. $S$ and $\sigma$ can then be calculated in terms of $s$ and $\eta$, where $\eta$ is a reduced chemical potential defined as $\eta = (E_F - E_t)/k_B T$ and represents the relative position of the Fermi level with respect to $E_t$ (see Supplementary Information Section F for more details).

The above model enables a fit for the $S$ versus $\sigma$ plot with two parameters: $s$ and $\sigma_{E_0}$. For PBTTT/F$_4$-TCNQ, $s = 3$ and $\sigma_{E_0} = (3 \pm 1) \times 10^{-2}$ Scm$^{-1}$ gave an excellent agreement with the data over the entire range as shown in Fig. 3b. For comparison, the mobility-edge model ($s = 0$) has a completely different curvature and could only fit the higher $\sigma$ range of the data (1-200 Scm$^{-1}$) (see Fig. 3b) but failed to describe the lower $\sigma$ range which is not self-consistent with an assumption of non-degenerate transport limit (i.e. $E_c - E_F << -k_B T$, where $E_c$ is the mobility-edge). This means that the mobility-edge model which predicts no $E$ dependence in $\sigma_E$ is not suitable for describing the charge transport in PBTTT/F$_4$-TCNQ. On the other hand, the good agreement with the $s = 3$ model suggests that the charge transport above the transport edge has a strong energy dependence. In addition, a narrow-band transport model which has been

employed for strongly-disordered systems [11, 14] yields a distinctly different $S$-$\sigma$ relationship to the $s = 3$ model. [31]

Here, we compare the PBTTT/ $F_4$-TCNQ results with other conducting polymers, CDT-BTZ and P3HT doped by solid-state diffusion of $F_4$-TCNQ (denoted as 'CDT-BTZ/$F_4$-TCNQ' and 'P3HT/$F_4$-TCNQ', respectively, from here). These polymers show orders of magnitude increase in conductivity with maximum conductivities of 63 Scm$^{-1}$ and 5.3 Scm$^{-1}$ upon solid-state doping with $F_4$-TCNQ [20], respectively. Our structural analysis based on XRD measurements (from our previous study [20]) and GID measurements (see Supplementary Information Section E) indicate that similar structural changes occur during the doping as PBTTT, except for slight differences in P3HT. In order to investigate their dependence of $S$ on $\sigma$, the same de-doping method was employed as described for PBTTT/$F_4$-TCNQ above. The changes in UV-Vis spectra during de-doping for both of the polymers are similar to those of PBTTT/$F_4$-TCNQ (see Supplementary Information Section E). The fit with the $s = 3$ model was found to be universal among these polymers, but with different $\sigma_{E_0}$. The $\sigma_{E_0}$ of CDT-BTZ/$F_4$-TCNQ and P3HT/$F_4$-TCNQ are determined to be $1.5 \times 10^{-2}$ Scm$^{-1}$ and $1.0 \times 10^{-3}$ Scm$^{-1}$, respectively; i.e. are smaller than $\sigma_{E_0}$ of PBTTT/$F_4$-TCNQ. $\sigma_{E_0}$ can be related to the intrinsic mobility of a system via the following general relation that can be derived for independent-electron systems by Kubo-formalism [32]

$$\frac{\partial \sigma_E(E,T)}{\partial E} = qg(E,T)\mu_E(E,T), \tag{3}$$

where $q$ is the elementary charge, $g(E,T)$ is the density of states (DOS) and $\mu_E(E,T)$ is the microscopic mobility of the states at $E$ at temperature $T$. The latter is an energy-dependent parameter that gives the average drift velocity of charges occupying the states at $E$, under an applied electric field. Note that we have assumed that the energy dependence of the terms in Eqn. 3 can be separated to their temperature dependence similarly to the definition of $\sigma_{E_0}$. In this study, only the energy dependence of the terms (i.e. $\sigma_E(E)$, $g(E)$ and $\mu_E(E)$) will be discussed. According to Eqn. 3, $\sigma_{E_0}$ is proportional to the $E$-independent prefactor of the product of $\mu_E$ and $g(E)$. Therefore, the higher $\sigma_{E_0}$ of PBTTT/$F_4$-TCNQ can be correlated with a significantly

higher intrinsic mobility of PBTTT/$F_4$-TCNQ compared to P3HT/$F_4$-TCNQ which also agrees with an order of magnitude higher FET mobility of PBTTT (maximum 1 cm$^2$/Vs) [33, 34] compared to P3HT ($<$ 0.1 cm$^2$/Vs) [35] reported in the literature. The same order of magnitude of $\sigma_{E_0}$ value of CDT-BTZ/$F_4$-TCNQ is consistent with the FET-mobility of CDT-BTZ reported in literature having similar to that of PBTTT (maximum 3-4 cm$^2$/Vs [36, 37]). The difference in the maximum conductivity between PBTTT/$F_4$-TCNQ and CDT-BTZ/$F_4$-TCNQ can be due to the lower free carrier concentration generated by doping in CDT-BTZ/$F_4$-TCNQ ($\eta = 11$ at $\sigma = 21$ Scm$^{-1}$) than PBTTT/$F_4$-TCNQ ($\eta = 18$ at $\sigma = 163$ Scm$^{-1}$) since $E_F$ lies closer to $E_t$ for CDT-BTZ/$F_4$-TCNQ than PBTTT/$F_4$-TCNQ.

We can infer from Eqn. 3 that $g(E)$ and $\mu_E$ give a crucial information towards the origin of the strong energy dependence of $\sigma_E$ observed in a wide range of conducting polymers. However, $\mu_E$ can not be directly measured (unlike the macroscopic mobility, $\mu$, given by $\sigma = ne\mu$) but can only be determined from knowing $\sigma_E$ and $g(E)$. Therefore, we can first make an attempt to determine $g(E)$ of PBTTT/$F_4$-TCNQ by correlating it with the charge concentration, N, at different doping levels (i.e. at different $E_F$) determined by electron spin resonance (ESR) measurements. The mathematical procedures for relating $g(E)$ to N is shown in details in Section G of Supplementary Information. In short, the Curie susceptibility determined from the ESR measurements gave an estimate of number of localized spins from $F_4$-TCNQ anions generated upon doping, N$_{spin}$, which can be approximated as the number of holes generated in PBTTT as demonstrated in previous studies [20, 38]. Figure 4a shows N versus $\eta$ data for the first four levels of de-doping measured for a PBTTT/$F_4$-TCNQ film following the same recipe as shown in Fig. 1a. $\eta$ for each N$_{spin}$ was determined from the $s = 3$ fit in Fig. 3b by inputting the conductivity values that were obtained after the same de-doping steps taken in Fig. 1a. The good agreement with the $s = 3$ model of $\sigma_E$ indicates that its components, $g(E)$ and $\mu_E(E)$ also exhibit power-law behavior in $E$. The DOS of PBTTT/$F_4$-TCNQ was formulated in the following form

$$g(E) = \begin{cases} g_i \times (E - E_t')^i & \text{for } E \geq E_t \\ g_L \times \exp(-(E_t - E)/\beta) & \text{for } E < E_t, \end{cases}$$

where the first case represents the DOS of mobile states that follow a power-law with an exponent, $i$, at energy above $E_t$ (i.e. $\eta > 0$), the second case is the DOS of localized states at energy below $E_t$ (i.e. $\eta < 0$), assuming that the DOS has a an exponential tail with a breadth of $\beta$. $g_i$ and $g_L$ are the prefactors to be determined when fitted to N versus $\eta$ data. Note that $E_t'$ is a modified $E_t$ according to the boundary conditions at $\eta = 0$, (see Section G, Supplementary Information for more details). The local component of the DOS was assumed to have a width of $\beta = 100$ meV which is an estimate based on previous studies in electrochemically doped polythiophenes at high doping levels [39]. Only the $i = 0$ and $i = 1/2$ models are shown since they gave good fits to the N $_{\text{spin}}$ versus $\eta$ data (see Fig. S8). The $i = 0$ model (i.e., a constant DOS at $E \geq E_t$) gave the best fit over the whole range of the data (black dashed line in Fig. 4a) with a fixed value of $g_0 = 5.6 \times 10^{20}$ eV$^{-1}$cm$^{-3}$ whereas the $i = 1/2$ model gave good fits within a finite window of $g_{1/2}$ from $1.3 \times 10^{21}$ eV$^{-1.5}$cm$^{-3}$ to $1.9 \times 10^{21}$ eV$^{-1.5}$cm$^{-3}$ (a light pink region). The corresponding DOS profiles for $i = 0$ and $i = 1/2$ models are shown in Fig. 4b along with the marked values of the DOS at $\eta$ of each N $_{\text{spin}}$ (shown as orange and black solid circles for $i = 0$ and $i = 1/2$, respectively).

Two scenarios can be postulated from the two models. Firstly, the $i = 1/2$ model could account for the dynamic nature of the DOS profile upon doping; the varying best fit with $g_{1/2} = 1.9 \times 10^{21}$ eV$^{-1.5}$cm$^{-3}$ for N $_{\text{spin}}$ at $\eta = 4.1$ and $g_{1/2} = 1.3 \times 10^{21}$ eV$^{-1.5}$cm$^{-3}$ for N $_{\text{spin}}$ at $\eta = 18.9$ may indicate a continuous transition of the DOS profile upon doping (indicated by the red block arrow in Fig. 4b). The decrease in $g_{1/2}$ could reflect the increase in the energetic disorder since the slope of the DOS at $E_F$ becomes shallower. A similar argument has been recently presented by Thomas et al. [40] who investigated a $i = 2$ power-law DOS model for an ionic-liquid gated PBTTT transistor. A continuous increase in the dopant anion concentration is expected to create additional energetic disorder via attractive Coulomb potential that would broaden the DOS profile [41, 42]. On the other hand, a good agreement with the $i = 0$ model over the entire range of the data implies a nearly static DOS profile upon doping. Although the static DOS profile over a wide range of doping levels may be an oversimplification, one could expect that the broadening effect of the DOS due to the additional dopants could play a little role at the heavily-doped limit [43, 41], especially in the range of N $_{\text{spin}}$ that we are

considering (between $\approx 1$ and $3 \times 10^{20}$ cm$^{-3}$). In the heavily-doped limit, the Coulomb potential wells created by F$_4$-TCNQ anions could have already significantly overlapped such that further addition of ionized dopants may not create new deep traps [41]. Arkihipov et al. showed for electrochemically doped P3HT that the width of the DOS stayed relatively constant above the doping level of 3% [43]. The doping level in PBTTT/F$_4$-TCNQ nearly reaches 20% at the maximum [20] (i.e. $N \approx 3 \times 10^{20}$ cm$^{-3}$). Moreover, the physical significance of a constant DOS above $E_t$ is that the model agrees well with the verified two-dimensional nature of the charge transport originating from a two-dimensional ordered lamella structure in PBTTT/F$_4$-TCNQ [20], as well as in other polythiophenes [35, 44].

Although the argument for the $i = 0$ model above remains qualitative, the good agreement of the model for N versus $\eta$ provides a useful insight for the $E$ dependence of $\mu_E$ via Eqn. 3. Since $\sigma_E$ behaves as $s = 3$, $\mu_E$ is expected to follow $\mu_E \propto (E - E_t)^2$ at $E \geq E_t$, assuming a constant $g(E)$ at $E \geq E_t$. Therefore, we expect that the intrinsic mobility of PBTTT/F$_4$-TCNQ is strongly energy-dependent at the heavily-doped limit and is expected to increase further with additional doping, as shown in Fig. 4c. The quadratic behavior of $\mu_E$ is non-trivial and the origin of the enhancement of mobility at high doping levels needs further investigation but the shrinkage of the $\pi$-$\pi$ stacking distance in PBTTT upon the solid-state doping, albeit small, could result in a greater interchain overlap integral, and therefore contributing to a sufficiently large charge delocalization which allows the observation of Hall effect and weak-localization [20]. A similar effect has been observed in poly(3-alkylthiophene) [28] and the larger charge delocalization in PBTTT/F$_4$-TCNQ is further supported by a recent observation of a longer phase-coherence length at higher doping levels [38]. The strong energy dependence of mobility is consistent with our experimental observation of the measured Hall mobility of $\approx 2$ cm$^2$/Vs in PBTTT/F$_4$-TCNQ [20] which is roughly a factor of 2 higher than the maximum FET mobility of PBTTT reported in literature [33, 34]. This could be due to a larger contribution of carriers occupying states up to higher $E$ with higher $\mu_E$ when heavily-doped. In addition, Fujimoto et al. [38] recently showed that the mobility of PBTTT/F$_4$-TCNQ decreased after de-doping via annealing which is consistent with our analysis. Moreover, the energy dependence of mobility has been observed in various other conducting

polymers - polyacetylene [45], polyaniline [46], polythiophenes [47, 48, 49, 50], poly-p-phenylene sulfide [51, 52] and recently in PEDOT [53]. Normally, the mobility enhancement at higher energy has been associated with insulator-metal transition via the generation of metallic bands by polarons and bipolarons [54]. In heavily doped PEDOT, the polaron band formation was found to be driven by a strong interchain interaction [53]. There is a question as to whether such phase transition can be incorporated into the current model. However, note that the formation of bipolarons would not be significant in PBTTT/F$_4$-TCNQ since the ESR signal intensity only increased upon doping which contradicts the spin-less nature of bipolarons, as measured previously. [55, 56]

Although the presented models provide a good fit to the data, some aspects of the fits may urge caution in the interpretation. According to the model, the conductivity range measured for PBTTT/F$_4$-TCNQ represents sweeping the $E_F$ from $6k_BT$ below $E_t$ (pristine PBTTT of $\sigma = 10^{-4}$ Scm$^{-1}$) to $19k_BT$ above $E_t$ (fully doped PBTTT of $\sigma = 200$ Scm$^{-1}$) which represents a transition from the non-degenerate semiconductor limit ($\eta \ll -1$) to degenerate semiconductor limit ($\eta \gg 1$). This wide energy range of conduction is in contrast with a conventional narrow-band transport in OSCs (typically below 500 meV [57]). The bandwidth of over 0.64 eV is not completely unreasonable considering theoretical values(over 0.7 eV in $\pi$-$\pi$ stacking direction of PBTTT [58, 59] and approximately 0.6 eV in P3HT [44]), although the calculations assume no backbone-tilting which would reduce the bandwidth significantly. In addition, the width of the localized tail states is not a parameter that can not be determined exactly from the model, given the range of the data available. Despite a relatively good fit that can be achieved with $\beta$ of 100 meV, the value of $\beta$ is roughly the same as what is expected from a paracrystalline disorder in PBTTT [60] and only slightly higher than the dipolar disorder due to charge-dipole interaction near the gate dielectric in FETs [23]. Although we can argue that the extra energetic disorder caused by the dopants plays a small role at very high doping levels, the effect of doping on the bandwidth and the degree of energetic disorder caused by the structural changes accompanied by the incorporation of the ionized dopants should be quantitatively analyzed from further works.

The thermoelectric properties of PBTTT/$F_4$-TCNQ and P3HT/$F_4$-TCNQ from the current work can be compared to other doping methods reported in literature to investigate the doping method dependence on the thermoelectric properties. As shown from Fig. 5a the dataset for solution-doped PBTTT by Glaudell et al. [16] lies along the $\sigma_{E_0} = 1.0 \times 10^{-3}$ Scm$^{-1}$ fit. This is an order of magnitude lower than that of PBTTT/$F_4$-TCNQ. This is in agreement with our results from the previous work [20] which demonstrated that the solid-state doping method perturbs the structural order of PBTTT less than the solution-doping method, which results in a higher mobility of $\approx 2$ cm$^2$/Vs. The presented work also shows a superior $\sigma_{E_0}$ to immersion-doping of PBTTT in a solution of ferric salt of triflimide anions TFSI $^-$[61] and 4-ethylbenzenesulfonic acid (EBSA) [62]. Recently, Patel et al. [62] showed that vapor-phase doping of PBTTT with (tridecafluoro-1,1,2,2-tetrahydrooctyl)trichlorosilane (FTS) could achieve the maximum conductivity of 1300 Scm$^{-1}$ and the Seebeck coefficient of $14\mu$V/K. The vapor-phase doping is technically similar to our solid-state doping in that the doping involves depositing FTS molecules in vapor phase on top of the polymer under low vacuum conditions [16, 62]. Although the dataset was limited, the data points for FTS-doped PBTTT agreed with fitting lines for $\sigma_{E_0}$ between $1.0 \times 10^{-3}$ Scm$^{-1}$ (for low $\sigma$) and $5.0 \times 10^{-3}$ Scm$^{-1}$ at high $\sigma$ (see Fig. 5a). This suggests that FTS-doped PBTTT may have a similar energy dependence of mobility as our PBTTT/$F_4$-TCNQ but exhibit a higher maximum conductivity due to a higher free carrier concentration generated ($\eta = 33$ for $\sigma = 1100$ Scm$^{-1}$) since FTS has a higher electron affinity of than F$_4$-TCNQ. A similar conclusion can be drawn for P3HT which shows a significantly higher maximum conductivity with FTS-doped P3HT (27.7 Scm$^{-1}$) [63] than our P3HT/$F_4$-TCNQ (3.51 Scm$^{-1}$) and solution-doped P3HT (0.18 Scm$^{-1}$) [16], although they could all be fitted reasonably with $\sigma_{E_0} = 1.0 \times 10^{-3}$ Scm$^{-1}$ (Fig. 5a). The similar values of $\sigma_{E_0}$ in P3HT upon doping may be due to similar structural changes induced by the two doping methods (Supplementary information Section E).

It is interesting to discuss how the thermoelectric properties discussed above can set guidelines for their thermoelectric power factors, $S^2\sigma$, which directly relates to their potential power conversion efficiencies. Two conclusions can be drawn from the plot of the power factor dependence on $\sigma$ shown in Fig. 5b. Firstly, the higher the $\sigma_{E_0}$, the higher the power factor for a

given conductivity. As discussed above, we therefore expect PBTTT/F$_4$-TCNQ to have the highest power (the maximum of $61.9 \pm 4.6 \mu\mathrm{Wm}^{-1}\mathrm{K}^{-2}$) out of the measured polymers due to a higher intrinsic mobility; maximum values of $10 \pm 2 \mu\mathrm{Wm}^{-1}\mathrm{K}^{-2}$ and $1.5 \pm 0.4 \mu\mathrm{Wm}^{-1}\mathrm{K}^{-2}$ for CDT-BTZ/F$_4$-TCNQ and P3HT/F$_4$-TCNQ, respectively. The maximum power factor of PBTTT/F$_4$-TCNQ is also 60 times higher than the value of $1.3 \mu\mathrm{Wm}^{-1}\mathrm{K}^{-2}$ for solution-doped PBTTT, as a result of the higher $\sigma_{\mathrm{E}_0}$. However, the maximum power factor of P3HT/F$_4$-TCNQ is still 5 times higher than that of solution-doped P3HT and even higher than solution-doped PBTTT [16] despite a similar $\sigma_{\mathrm{E}_0}$. This leads to the second conclusion that can be drawn within the framework of the $s = 3$ model, which predicts that the higher the $\eta$, the higher the power factor. Therefore, there is a gain in the power factor by generating a higher free carrier concentration. This is possibly related to the larger contribution of charges occupying states with higher $\mu_{\mathrm{E}}$ as $\eta$ increases, which would increase $\sigma$ significantly to compensate for the decrease in $S^2$, according to Eqn. 1. The trend is in contrast with a conventional parabolic band, energy-independent scattering model for metals and degenerate semiconductors [64] which predicts that the power factor decreases if the carrier concentration is greater than an optimum value.

The trend from the compiled results clearly shows that there is a room for optimization by employing a doping method which preserves the structural order of the polymer (to result in a high $\sigma_{\mathrm{E}_0}$) and generates a high free carrier concentration (i.e. a high $\eta$). This is supported by the high power factors achieved in PBTTT doped by the solid-state doping with F$_4$-TCNQ. The fit for $\sigma_{\mathrm{E}_0} = 3.0 \times 10^{-2}$ Scm$^{-1}$ also predicts a potential gain in the power factor if we can further increase the free carrier concentration, assuming the model holds the same at higher doping levels. If the conductivity could reach, for example, 2000 Scm$^{-1}$ by filling states up to $\eta = 40$, the expected power factor is $88 \, \mu\mathrm{Wm}^{-1}\mathrm{K}^{-2}$. To improve beyond this, we should achieve higher $\eta$ by using stronger dopants than F$_4$-TCNQ, since when fully doped, not all the F$_4$-TCNQ molecules incorporated in PBTTT undergo charge-transfer [20]. In this respect, FTS may be a suitable candidate as a dopant. As shown in Fig. 5b, the maximum power factor reported for FTS-doped PBTTT is $110 \pm 34 \, \mu\mathrm{Wm}^{-1}\mathrm{K}^{-2}$ [62] and $10 \pm 3 \mu\mathrm{Wm}^{-1}\mathrm{K}^{-2}$ for P3HT [16]. These high values can be attributed to a higher free carrier concentration than, and as high $\sigma_{\mathrm{E}_0}$

as that can be achieved with our solid-state doping with $F_4$-TCNQ. Assuming that the $i = 0$ model holds for the DOS at $\eta = 33$, the predicted carrier concentration is approximately $5 \times 10^{21}\,\mathrm{cm}^{-3}$, with the predicted $\mu \approx 13$ cm$^2$/Vs. There is a question as to how far we can increase the charge concentration before reaching the maximum limit. The charge density of $10^{21}\,\mathrm{cm}^{-3}$ reflects the same order as the PBTTT repeat unit density using the measured $\pi$ spacing, out-of-plane d-spacing and unit-cell parameters for PBTTT [25]. However, the predicted power factor at this charge concentration ($\eta = 66$, assuming the $i = 0$ model) is approximately $140\,\mu\mathrm{Wm}^{-1}\mathrm{K}^{-2}$ which is still relatively low compared to the record value of $460\,\mu\mathrm{Wm}^{-1}\mathrm{K}^{-2}$ for PEDOT:Tos [10]. Therefore, to realistically improve the power factor of PBTTT, rather than merely increasing carrier concentration, we need to develop a doping method (and dopants) which enhances $\sigma_{E_0}$ by reducing further the amount of structural and energetic disorder associated with the dopant incorporation. The importance of polymer film morphology on the thermoelectric properties has not been discussed extensively in the literature. Recent works have shown the importance of the orientational correlation length of polymer backbones on thermoelectric power factor [63] and improved thermoelectric power factor upon chain alignment by a high-temperature mechanical rubbing process [65]. The degree of chain orientation is a parameter that can be potentially incorporated in $\sigma_{E_0}$ of the model studied here (e.g. the data for $S$ and $\sigma$ of the aligned P3HT doped by $F_4$-TCNQ [65] can be placed near the $s = 3$ and $\sigma_{E_0} = 5.0 \times 10^{-3}$ Scm$^{-1}$ line).

Achieving the doping level near the maximum charge density of $\approx 10^{21}\,\mathrm{cm}^{-3}$ (as discussed above) would not be only challenging but would probably introduce formation of bipolarons which will drastically change the charge transport, as well as their thermoelectric properties. Indeed, the formation of a semi-metallic bipolaron band at high doping levels was discovered to be the origin of a unusually high thermoelectric power factor in PEDOT:Tos [10]. Kang et al. [19] hinted that the unique charge transport properties of PEDOT:Tos were reflected in the variation of $S$ with $\sigma$ which could be fitted to $s = 1$ curves unlike all other conducting polymers (well-fitted with $s = 3$). Therefore, there is a scope for searching potential material systems which would show different power-law energy-dependence of $\sigma_E$, while having a high $\sigma_{E_0}$ (75 Scm$^{-1}$ for PEDOT:Tos [19]). However, the big gap in the power factor values of the

polymers discussed in this work and PEDOT:Tos may not entirely come from superior intrinsic charge transport properties in PEDOT:Tos. There are also structural differences between the conducting polymers that we have presented and PEDOT:Tos in terms of packing density of polymer chains. Especially, in light of the two-dimensional nature of the transport in PBTTT/$F_4$-TCNQ as demonstrated in our previous work [20], it may be helpful to consider an effective conductivity of each two-dimensional layer in which the actual charge transport occurs (i.e. it excludes the side-chains which are insulating). The interdigitated side-chains take up a significant volume (roughly 3/4 of the thickness, considering the effective thickness taken by the core polymer backbone of around 5Å). Therefore, the effective conductivity of each polymer backbone layer is estimated to be in the order of 1000 Scm$^{-1}$, which would also mean these layers would contribute to the total effective thermoelectric power factor of around $250\ \mu\mathrm{Wm^{-1}K^{-2}}$. This assumes that the Seebeck voltage which is generated by the individual conducting layers that are connected electrically in parallel would not change if it was possible to remove the insulating side chains from the film. Although this consideration is not practically relevant, this suggests that at least some of the inferior thermoelectric performance of the polymers used here compared to PEDOT:Tos can be attributed to the dilution of the conducting polymer by the solubilizing but insulating side-chains. Finally, our power factor discussion should be complemented with future studies on the effect of doping on the thermal conductivity of the conducting polymers in order to ultimately determine the optimal level of doping that maximizes the thermoelectric power efficiency, $zT$. It is possible that the level of doping that we achieved with solid-state diffusion is close to the optimum state for $zT$ considering a potential increase in the electronic contribution of the thermal conductivity at high doping levels ($\sigma$ above 200 Scm$^{-1}$) as reported for PEDOT:Tos. [66] Therefore, the controllability of the thermoelectric response by the simple de-doping technique demonstrated here would be a crucial step towards optimizing $zT$ for developing high-efficiency organic thermoelectric generators.

# 3  Conclusion

Our results show that conjugated polymers efficiently doped by solid-state diffusion of $F_4$-TCNQ could be controllably de-doped via post-process thermal annealing to enable a systematic study of the thermoelectric properties of various materials in a wide range of doping levels. The optical measurements showed that the de-doping occurs via a continuous diffusion of $F_4$-TCNQ molecules out of the film during annealing to reduce the number of dopants in the polymer film available for charge-transfer, inducing a structural change in the film in a continuous fashion with no sign of phase-segregation of the crystallites of the polymer until the structure recovers back to a pristine state (fully de-doped). The same power-law of energy dependence of the transport function could be used to predict the thermoelectric properties of PBTTT, CDT-BTZ and P3HT in the wide range of doing levels. The strong energy dependence of the transport function was shown to originate from the energy-dependence of the microscopic mobility. Two key parameters can be drawn from the comparison of thermoelectric properties of the polymers in achieving high thermoelectric power factors in conducting polymers: the system needs to have a high intrinsic mobility (reflected by a large effective transport coefficient) and the system needs to be doped efficiently to access higher energy states with a higher microscopic mobility which contribute towards a higher electrical conductivity. PBTTT doped via solid state diffusion of $F_4$-TCNQ is a useful model system where both can be satisfied to achieve a relatively high thermoelectric power factor.

### Experimental Section

### Materials

PBTTT-C$_{14}$ was synthesized and purified via a standard Stille copolymerization [33] where number average molecular weight and polydispersity were measured to be 30 kDa and 1.4. The molecular weight was determined by Agilent Technologies 1200 series GPC running in chlorobenzene at 80  , using two PL mixed B columns in series, and calibrated against narrow polydispersity polystyrene standards.

### Device fabrication

For the fabrication of the devices, a glass substrate was cleaned via sonication with deionized water, acetone and isopropanol. After the cleaning with an oxygen plasma treatment, electrodes were defined by photolithography and deposited via thermal evaporation of Ti/Au (7 nm/ 18 nm) at the base pressure of $9 \times 10^{-7}$ mbar. The details of the device architecture for the Hall-bar device (for 4-point probe conductivity measurement) is described in our previous work [20] and the multi-functional device architecture (shown in Fig. 3a) is described in the Supplementary Information Section A. PBTTT film was spin-coated on top of the electrodes from a solution with the concentration of 10 mg ml$^{-1}$ dissolved in 1,2-dichlorobenzene in a nitrogen glovebox to form a 40 nm thick film (1500 rpm for 60 seconds), which was annealed at 180 ˚C for 20 mins, then slowly cooled down to room temperature to form a terrace phase. The F$_4$-TCNQ was thermally evaporated on the top of the PBTTT film (purchased from Sigma-Aldrich) at a pressure of $1 \times 10^{-6}$ mbar at the rate of 0.5 Å s$^{-1}$ up to a nominal thickness of 20 nm. To complete the doping procedure, the doped film was annealed at 80 ˚C for 20 minutes. The doped film was then patterned by combination of photolithography with etching by oxygen plasma. More details are given in Supplementary information Section A and B. The samples for UV-Vis and X-ray measurements were also made in the same condition as for the PBTTT and F$_4$-TCNQ deposition as described above.

**Acknowledgements**

**Additional information**

The authors declare no competing financial interests.

# References

[1]   G Jeffrey Snyder and Eric S Toberer.   Complex thermoelectric materials.   *Nature Materials*, 7(2):105–114, February 2008.

[2]   Cronin B Vining.   An inconvenient truth about thermoelectrics.   *Nature Materials*, 8(2):83–85, February 2009.

[3]   Xu Xie, Dongyao Li, Tsung-Han Tsai, Jun Liu, Paul V Braun, and David G Cahill. Thermal Conductivity, Heat Capacity, and Elastic Constants of Water-Soluble Polymers and Polymer Blends.   *Macromolecules*, 49(3):972–978, February 2016.

[4]   Yuji Hiroshige, Makoto Ookawa, and Naoki Toshima.   Thermoelectric figure-of-merit of iodine-doped copolymer of phenylenevinylene with dialkoxyphenylenevinylene.   *Synthetic Metals*, 157(10-12):467–474, June 2007.

[5]   Hye Jeong Lee, Gopinathan Anoop, H J Lee, Hyeon Jun Lee, Chingu Kim, Ji-Woong Park, Jaeyoo Choi, Heesuk Kim, Yong-Jae Kim, Eunji Lee, Sang-Gil Lee, Young-Min Kim, Joo-Hyoung Lee, and Ji Young Jo.   Enhanced thermoelectric performance of PEDOT:PSS/PANI–CSA polymer multilayer structures.   *Energy & Environmental Science*, 9(9):2806–2811, 2016.

[6]   Jian Liu, Li Qiu, Giuseppe Portale, Marten Koopmans, Gert Ten Brink, Jan C Hummelen, and L Jan Anton Koster.   N-Type Organic Thermoelectrics: Improved Power Factor by Tailoring Host-Dopant Miscibility.   *Advanced Materials*, 29(36):1701641, September 2017.

[7]   Hideki Ueno and Katsumi Yoshino.   Electrical conductivity and thermoelectric power of highly graphitizable poly(p-phenylene vinylene) films.   *Physical review. B, Condensed matter*, 34(10):7158–7163, November 1986.

[8] Olga Bubnova, Zia Ullah Khan, Abdellah Malti, Slawomir Braun, Mats Fahlman, Magnus Berggren, and Xavier Crispin. Optimization of the thermoelectric figure of merit in the conducting polymer poly(3,4-ethylenedioxythiophene). *Nature materials*, 10(6):429–33, jul 2011.

[9] G H Kim, L Shao, K Zhang, and K P Pipe. Engineered doping of organic semiconductors for enhanced thermoelectric efficiency. *Nature Materials*, 12(8):719–723, August 2013.

[10] Olga Bubnova, Zia Ullah Khan, Hui Wang, Slawomir Braun, Drew R Evans, Manrico Fabretto, Pejman Hojati-Talemi, Daniel Dagnelund, Jean-Baptiste Arlin, Yves H Geerts, Simon Desbief, Dag W Breiby, Jens W Andreasen, Roberto Lazzaroni, Weimin M Chen, Igor Zozoulenko, Mats Fahlman, Peter J Murphy, Magnus Berggren, and Xavier Crispin. Semi-metallic polymers. *Nature materials*, 13(33):190–4, 2014.

[11] Deepak Venkateshvaran, Mark Nikolka, Aditya Sadhanala, Vincent Lemaur, Mateusz Zelazny, Michal Kepa, Michael Hurhangee, Auke Jisk Kronemeijer, Vincenzo Pecunia, Iyad Nasrallah, Igor Romanov, Katharina Broch, Iain McCulloch, David Emin, Yoann Olivier, Jérôme Cornil, David Beljonne, and Henning Sirringhaus. Approaching disorder-free transport in high-mobility conjugated polymers. *Nature*, 515(7527):384–388, November 2014.

[12] D Venkateshvaran, a J Kronemeijer, J Moriarty, D Emin, and H Sirringhaus. Field-effect modulated Seebeck coefficient measurements in an organic polymer using a microfabricated on-chip architecture. *APL Materials*, 2(3):032102, March 2014.

[13] K P Pernstich, B Rössner, and B Batlogg. Field-effect-modulated Seebeck coefficient in organic semiconductors. *Nature Materials*, 7(4):321–325, April 2008.

[14] W Chr Germs, K Guo, R A J Janssen, and M Kemerink. Unusual Thermoelectric Behavior Indicating a Hopping to Bandlike Transport Transition in Pentacene. *Physical*

*Review Letters*, 109(1):016601, July 2012.

[15]   C N Warwick, D Venkateshvaran, and H Sirringhaus.   Accurate on-chip measurement of the Seebeck coefficient of high mobility small molecule organic semiconductors.   *APL Materials*, 3(9):096104, September 2015.

[16]   Anne M Glaudell, Justin E Cochran, Shrayesh N Patel, and Michael L Chabinyc.   Impact of the Doping Method on Conductivity and Thermopower in Semiconducting Polythiophenes. *Advanced Energy Materials*, 5(4):n/a–n/a, February 2015.

[17]   Deepak Venkateshvaran, Katharina Broch, Chris N Warwick, and Henning Sirringhaus. Thermoelectric transport properties of high mobility organic semiconductors.   *SPIE Organic Photonics + Electronics*, 9943:99430U–99430U–10, September 2016.

[18]   David Emin.   *Polarons*.   Cambridge University Press, 2013.

[19]   Stephen Dongmin Kang and G Jeffrey Snyder.   Charge-transport model for conducting polymers.   *Nature Materials*, 16(2):252–257, February 2017.

[20]   Keehoon Kang, Shun Watanabe, Katharina Broch, Alessandro Sepe, Adam Brown, Iyad Nasrallah, Mark Nikolka, Zhuping Fei, Martin Heeney, Daisuke Matsumoto, Kazuhiro Marumoto, Hisaaki Tanaka, Shin-Ichi Kuroda, and Henning Sirringhaus.   2D coherent charge transport in highly ordered conducting polymers doped by solid state diffusion.   *Nature Materials*, 15(8):896–902, August 2016.

[21]   Dean M DeLongchamp, R Joseph Kline, Youngsuk Jung, Eric K Lin, Daniel a Fischer, David J Gundlach, Sarah K Cotts, Andrew J Moad, Lee J Richter, Michael F Toney, Martin Heeney, and Iain McCulloch.   Molecular Basis of Mesophase Ordering in a Thiophene-Based Copolymer.   *Macromolecules*, 41(15):5709–5715, July 2008.

[22]   Justin E Cochran, Matthias JN Junk, AM Glaudell, P Levi Miller, John S Cowart, Michael

F Toney, Craig J Hawker, Bradley F Chmelka, and Michael L Chabinyc. Molecular interactions and ordering in electrically doped polymers: Blends of PBTTT and F4-TCNQ. *Macromolecules*, 47(19):6836–6846, 2014.

[23] N. Zhao, Y.-Y. Noh, J.-F. Chang, M. Heeney, I. McCulloch, and H. Sirringhaus. Polaron Localization at Interfaces in High-Mobility Microcrystalline Conjugated Polymers. *Advanced Materials*, 21(37):3759–3763, oct 2009.

[24] P. Pingel and D. Neher. Comprehensive picture of $p$-type doping of P3HT with the molecular acceptor F$_4$-TCNQ. *Physical Review B*, 87(11):115209, mar 2013.

[25] Eunkyung Cho, R Joseph Kline, Chad Risko, Dongwook Kim, Roman Gysel, Nichole Cates Miller, Dag W Breiby, Michael D McGehee, Michael F Toney, and Jean-Luc Brédas. Three-dimensional packing structure and electronic properties of biaxially oriented poly(2,5-bis(3-alkylthiophene-2-yl)thieno[3,2-b]thiophene) films. *Journal of the American Chemical Society*, 134(14):6177–6190, April 2012.

[26] TJ Prosa, MJ Winokur, J Moulton, P Smith, and AJ Heeger. X-ray-diffraction studies of the three-dimensional structure within iodine-intercalated poly(3-octylthiophene). *Physical review. B, Condensed matter*, 51(1):159–168, January 1995.

[27] Kohji Tashiro, Masamichi Kobayashi, Tsuyoshi Kawai, and Katsumi Yoshino. Crystal structural change in poly(3-alkyl thiophene)s induced by iodine doping as studied by an organized combination of X-ray diffraction, infrared/Raman spectroscopy and computer simulation techniques. *Polymer*, 38(12):2867–2879, June 1997.

[28] Tsuyoshi Kawai, Masahiro Nakazono, and Katsumi Yoshino. Effects of doping on the crystal structure of poly(3-alkylthiophene). *Journal of Materials Chemistry*, 2(9):903–906, 1992.

[29]    Jun Li, Correy Koshnick, Souleymane O Diallo, Sophia Ackling, David M Huang, Ian E Jacobs, Thomas F Harrelson, Kunlun Hong, Guangwu Zhang, Joseph Beckett, Mark Mascal, and Adam J Moule.    Quantitative Measurements of the Temperature-Dependent Microscopic and Macroscopic Dynamics of a Molecular Dopant in a Conjugated Polymer.    *Macromolecules*, 50(14):5476–5489, July 2017.

[30]    H Fritzsche.    A general expression for the thermoelectric power.    *Solid State Communications*, 9(21):1813–1815, November 1971.

[31]    Stephen Dongmin Kang, Maxwell Dylla, and G Jeffrey Snyder. Thermopower-conductivity relation for distinguishing transport mechanisms: Polaron hopping in CeO2 and band conduction in SrTiO3.    *Physical Review B*, 97(23):131, June 2018.

[32]    M H Cohen, E N Economou, and C M Soukoulis.    Bipolarons in disordered media. *Physical Review B*, 29(8):4500–4504, April 1984.

[33]    Iain McCulloch, Martin Heeney, Clare Bailey, Kristijonas Genevicius, Iain Macdonald, Maxim Shkunov, David Sparrowe, Steve Tierney, Robert Wagner, Weimin Zhang, Michael L Chabinyc, R Joseph Kline, Michael D McGehee, and Michael F Toney.    Liquid-crystalline semiconducting polymers with high charge-carrier mobility.    *Nature Materials*, 5(4):328–33, apr 2006.

[34]    Mi Jung Lee, Dhritiman Gupta, Ni Zhao, Martin Heeney, Iain McCulloch, and Henning Sirringhaus.    Anisotropy of Charge Transport in a Uniaxially Aligned and Chain-Extended, High-Mobility, Conjugated Polymer Semiconductor.    *Advanced Functional Materials*, 21(5):932–940, mar 2011.

[35]    H Sirringhaus, P J Brown, R H Friend, M M Nielsen, K Bechgaard, B M W Langeveld-Voss, A J H Spiering, R A J Janssen, E W Meijer, P Herwig, and D M de Leeuw.

Two-dimensional charge transport in self-organized, high-mobility conjugated polymers. *Nature*, 401(6754):685–688, October 1999.

[36]   Hoi Nok Tsao, Don M Cho, Insun Park, Michael Ryan Hansen, Alexey Mavrinskiy, Do Y Yoon, Robert Graf, Wojciech Pisula, Hans Wolfgang Spiess, and Klaus Müllen.   Ultrahigh mobility in polymer field-effect transistors by design.   *Journal of the American Chemical Society*, 133(8):2605–2612, March 2011.

[37]   Wojciech Pisula, Suhao Wang, Michael Kappl, Ingo Liebewirth, Maren Müller, Katrin Kirchhoff, and Klaus Müllen.   Organic field-effect transistors based on highly ordered single polymer fibers.   *Advanced Materials*, 24(3):417–420, January 2012.

[38]   Ryo Fujimoto, Shun Watanabe, Yu Yamashita, Junto Tsurumi, Hiroyuki Matsui, Tomokatsu Kushida, Chikahiko Mitsui, Hee Taek Yi, Vitaly Podzorov, and Jun Takeya. Control of molecular doping in conjugated polymers by thermal annealing.   *Organic Electronics*, 47:139–146, August 2017.

[39]   V. Arkhipov, E. Emelianova, P. Heremans, and H. Bässler.   Analytic model of carrier mobility in doped disordered organic semiconductors.   *Physical Review B*, 72(23):235202, dec 2005.

[40]   Elayne M Thomas, Bhooshan C Popere, Haiyu Fang, Michael L Chabinyc, and Rachel A Segalman.   Role of Disorder Induced by Doping on the Thermoelectric Properties of Semiconducting Polymers.   *Chemistry of Materials*, 30(9):2965–2972, May 2018.

[41]   V. Arkhipov, P. Heremans, E. Emelianova, and H. Bässler.   Effect of doping on the density-of-states distribution and carrier hopping in disordered organic semiconductors. *Physical Review B*, 71(4):045214, jan 2005.

[42]   Hassan Abdalla, Guangzheng Zuo, and Martijn Kemerink.   Range and energetics of

charge hopping in organic semiconductors. *Physical Review B*, 96(24):241202, December 2017.

[43]   V I Arkhipov, P Heremans, E V Emelianova, G J Adriaenssens, and H Bässler.   Charge carrier mobility in doped semiconducting polymers. *Applied Physics Letters*, 82(19):3245, 2003.

[44]   R. Street, J. Northrup, and A. Salleo.   Transport in polycrystalline polymer thin-film transistors. *Physical Review B*, 71(16):165202, apr 2005.

[45]   Y W Park, a J Heeger, M A Druy, and a G MacDiarmid.   Electrical Transport in Doped Polyacetylene. *Journal of Chemical Physics*, 73(2):946–957, 1980.

[46]   R Patil, Y Harima, K Yamashita, K Komaguchi, Y Itagaki, and M Shiotani.   Charge carriers in polyaniline film: a correlation between mobility and in-situ ESR measurements. *Journal of Electroanalytical Chemistry*, 518(1):13–19, 2002.

[47]   Y Harima, T Eguchi, and K Yamashita.   Enhancement of carrier mobilities in poly(3-methylthiophene) by an electrochemical doping. *Synthetic Metals*, 95(1):69–74, 1998.

[48]   Keiichi Kaneto, Shigenori Hayashi, Shogo Ura, and Katsumi Yoshino.   ESR and Transport Studies in Electrochemically Doped Polythiophene Film. *Journal of the Physical Society of Japan*, 54(3):1146–1153, March 1985.

[49]   Shigenori Hayashi, Keiichi Kaneto, Katsumi Yoshino, Rokuji Matsushima, and Tomochika Matsuyama.   Electrical Conductivity and ESR Studies in Iodine-Doped Polythiophene from Semiconductor to Metallic Regime. *Journal of the Physical Society of Japan*, 55(6):1971–1980, June 1986.

[50]   X Jiang, Y Harima, K Yamashita, Y Tada, J Ohshita, and A Kunai.   Doping-induced change of carrier mobilities in poly(3-hexylthiophene) films with different stacking structures.

*Chemical Physics Letters*, 364(5-6):616–620, October 2002.

[51]   Mun Soo Yun and Katsumi Yoshino.   Doping effect on carrier mobility in poly-p-phenylenesulfide.   *Journal of Applied Physics*, 58(5):1950–1954, September 1985.

[52]   C Tanase, P W M Blom, P Blom, D M de Leeuw, and D de Leeuw.   Origin of the enhanced space-charge-limited current in poly( p-phenylene vinylene).   *Physical Review B*, 70(19):193202, November 2004.

[53]   Jing-Mei Zhuo, Li-Hong Zhao, Perq-Jon Chia, Wee-Sun Sim, Richard Friend, and Peter K. Ho.   Direct Evidence for Delocalization of Charge Carriers at the Fermi Level in a Doped Conducting Polymer.   *Physical Review Letters*, 100(18):186601, may 2008.

[54]   J L Brédas, B Thémans, J G Fripiat, J M André, and R R Chance.   Highly conducting polyparaphenylene, polypyrrole, and polythiophene chains: An ab initiostudy of the geometry and electronic-structure modifications upon doping.   *Physical review. B, Condensed matter*, 29(12):6761–6773, June 1984.

[55]   M Nechtschein, F Devreux, F Genoud, E Vieil, J M Pernaut, and E Genies.   Polarons, bipolarons and charge interactions in polypyrrole: Physical and electrochemical approaches. *Synthetic Metals*, 15(1):59–78, June 1986.

[56]   F Devreux, F Genoud, M Nechtschein, and B Villeret.   ESR investigation of polarons and bipolarons in conducting polymers:: the case of polypyrrole.   *Synthetic Metals*, 18(1-3):89–94, February 1987.

[57]   Heinz Bässler and Anna Köhler.   Charge transport in organic semiconductors.   *Topics in current chemistry*, 312(Chapter 218):1–65, 2012.

[58]   D. M. DeLongchamp, R. J. Kline, E. K. Lin, D. A. Fischer, L. J. Richter, L. A. Lucas, M. Heeney, I. McCulloch, and J. E. Northrup.   High Carrier Mobility Polythiophene Thin Films:

Structure Determination by Experiment and Theory. *Advanced Materials*, 19(6):833–837, mar 2007.

[59] John Northrup. Atomic and electronic structure of polymer organic semiconductors: P3HT, PQT, and PBTTT. *Physical Review B*, 76(24):245202, dec 2007.

[60] J Rivnay, R Noriega, J E Northrup, R J Kline, and MF Toney B. Structural origin of gap states in semicrystalline polymers and the implications for charge transport. *Physical Review B*, 83(12):121306–4, 2011.

[61] Qian Zhang, Yimeng Sun, Wei Xu, and Daoben Zhu. What To Expect from Conducting Polymers on the Playground of Thermoelectricity: Lessons Learned from Four High-Mobility Polymeric Semiconductors. *Macromolecules*, 47(2):609–615, jan 2014.

[62] Shrayesh N Patel, Anne M Glaudell, David Kiefer, and Michael L Chabinyc. Increasing the Thermoelectric Power Factor of a Semiconducting Polymer by Doping from the Vapor Phase. *ACS Macro Letters*, 5(3):268–272, February 2016.

[63] Shrayesh N Patel, Anne M Glaudell, Kelly A Peterson, Elayne M Thomas, Kathryn A O'Hara, Eunhee Lim, and Michael L Chabinyc. Morphology controls the thermoelectric power factor of a doped semiconducting polymer. *Science Advances*, 3(6):e1700434, June 2017.

[64] M Cutler, J F Leavy, and R L Fitzpatrick. Electronic Transport in Semimetallic Cerium Sulfide. *Physical Review*, 133(4A):A1143–A1152, February 1964.

[65] Amer Hamidi-Sakr, Laure Biniek, Jean-Louis Bantignies, David Maurin, Laurent Herrmann, Nicolas Leclerc, Patrick Lévêque, Vishnu Vijayakumar, Nicolas Zimmermann, and Martin Brinkmann. A Versatile Method to Fabricate Highly In-Plane Aligned Conducting Polymer Films with Anisotropic Charge Transport and Thermoelectric Properties: The Key Role of Alkyl Side Chain Layers on the Doping Mechanism. *Advanced Functional Materials*,

27(25):1700173, May 2017.

[66]   Annie Weathers, Zia Ullah Khan, Robert Brooke, Drew Evans, Michael T Pettes, Jens Wenzel Andreasen, Xavier Crispin, and Li Shi.   Significant Electronic Thermal Transport in the Conducting Polymer Poly(3,4-ethylenedioxythiophene).   *Advanced Materials*, 27(12):2101–2106, March 2015.
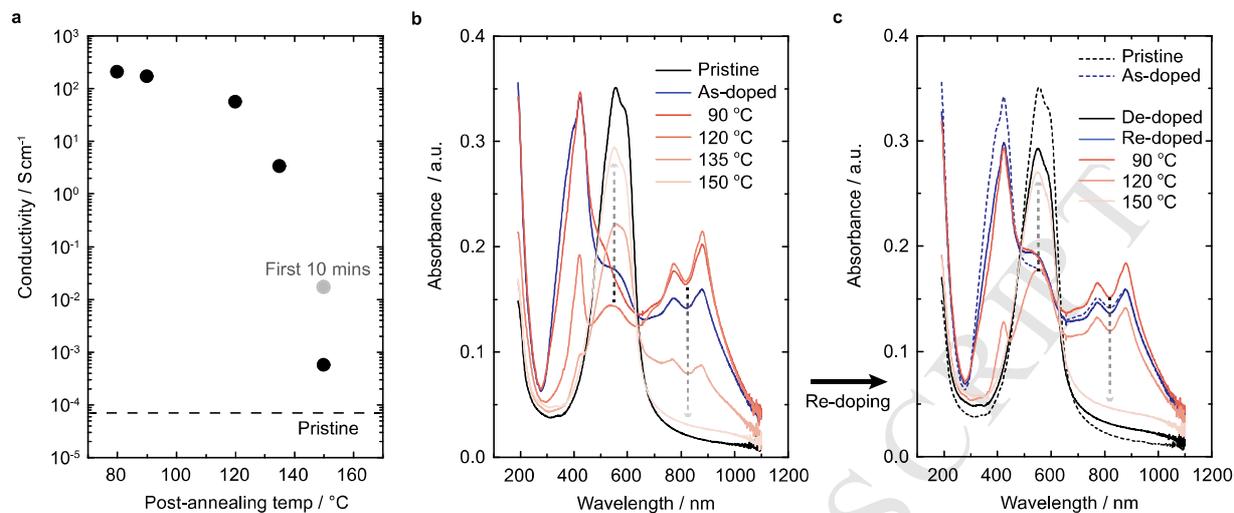
Figure 1: **Controllable de-doping of PBTTT/F4-TCNQ via post-process annealing.**
**a**, The measured conductivity as fully doped PBTTT/$F_4$-TCNQ film gets annealed for 20 minutes at each temperature, consecutively. The grey data point represents the conductivity of the sample measured after the first 10 minutes of annealing at 150 ℃. The doping/de-doping method presented in this work can achieve a controllable doping over 6 orders of magnitude conductivity range nearly down to the conductivity of a pristine sample (dashed line). **b**, UV-Vis absorption of the film plotted at each stage of de-doping: before doping (black), straight after doping (blue) and after annealing at each indicated temperature for 20 minutes (different strengths of red). The bleached neutral absorption after doping recovers (up-dashed-arrow near 555nm) whereas the absorption of $F_4$-TCNQ anions at 767 and 869 nm diminishes (down-dashed-arrow). **c**, The de-doped film (after 150 ℃ shown in **b**, shown as a black line) could be re-doped (blue) and then de-doped again via annealing consecutively at each temperature (different strengths of red). Similar trends occur while de-doping like in **b**. The spectra measured for the film in a pristine (dashed black line) and as-doped (dashed blue line) state are drawn for comparison.
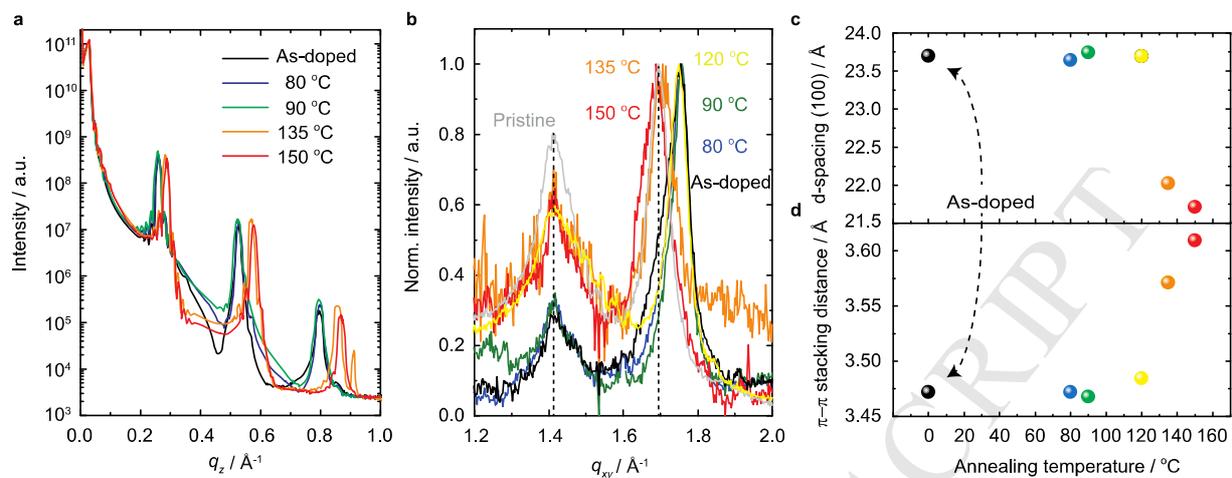
Figure 2: **XRD and GID patterns in PBTTT/F$_4$-TCNQ in the de-doping process.**

**a**, XRD patterns along the out-of-plane scattering direction, $q_z$, for samples annealed through the same de-doping cycle as described in Fig. 1. **b**, GID patterns along the in-plane direction, $q_{xy}$, which shows two peaks, at $1.41\text{Å}^{-1}$ and around $1.70\text{Å}^{-1}$ for a pristine sample (grey), as-doped sample (black), samples annealed at each different temperature (shown in the legend) for 20 minutes, consecutively. The dashed lines show the peak positions for the pristine PBTTT. **c**, The extracted lamellar d-spacings determined from the (300) peaks in **a** which suffer the least from the $1/q$ background signal from reflection. The spacing for the 'as-doped' sample is 23.4Å which remains constant until the 120 ℃ step after which the lamellar spacing decreases gradually to 21.7Å. **d**, $\pi$-$\pi$ stacking distance determined from **b** decreases to 3.47Å upon doping and gradually recovers to that of the pristine sample.
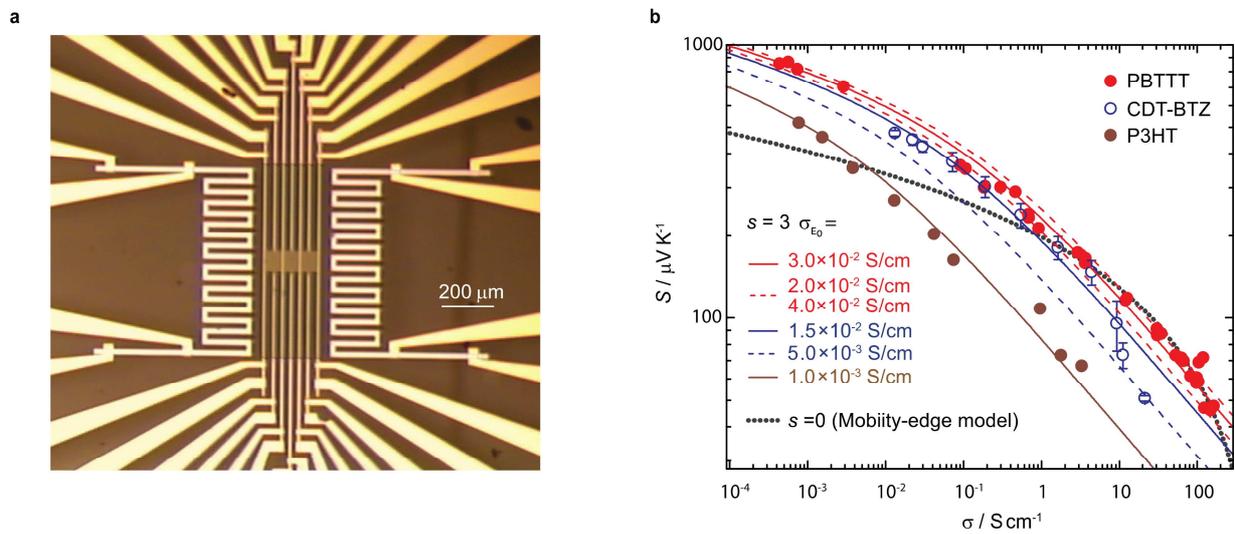
Figure 3: **Thermoelectric measurements of conducting polymers doped by solid-state doping. a**, Optical micrograph of the multi-functional device which enables an accurate measurement of Seebeck coefficient, $S$, and conductivities, $\sigma$ in the same film. The scale bar represents $200\mu$m. **b**, Comparison of $S$ versus $\sigma$ variation for PBTTT (red solid circles), CDT-BTZ (blue hollow circles) and P3HT (brown solid circles) doped with $F_4$-TCNQ with the solid-state doping method. For PBTTT, $S$ and $\sigma$ for three devices (shown in **a**) were measured at each de-doping step with the same device. The variation of $S$ vs $\sigma$ is best described by a energy-dependent mobility model by Kang et al. [19] with $s = 3$ and $\sigma_{E_0} = 3 \times 10^{-2}$ Scm$^{-1}$ (solid red line) with an error bound drawn as red-dashed lines for $\sigma_{E_0} = 2 \times 10^{-2}$ Scm$^{-1}$ and $\sigma_{E_0} = 4 \times 10^{-2}$ Scm$^{-1}$. The $s = 0$ fit (black dotted line) is drawn for comparison. The $s = 3$ model also produces good fits for the two other polymers with different values of $\sigma_{E_0}$ as $1.5 \times 10^{-2}$ Scm$^{-1}$ (blue solid line) and $1.0 \times 10^{-3}$ Scm$^{-1}$ (brown solid line) for CDT-BTZ and P3HT, respectively. The error bars represent the measurement error due to the device variation which was only significant for CDT-BTZ.
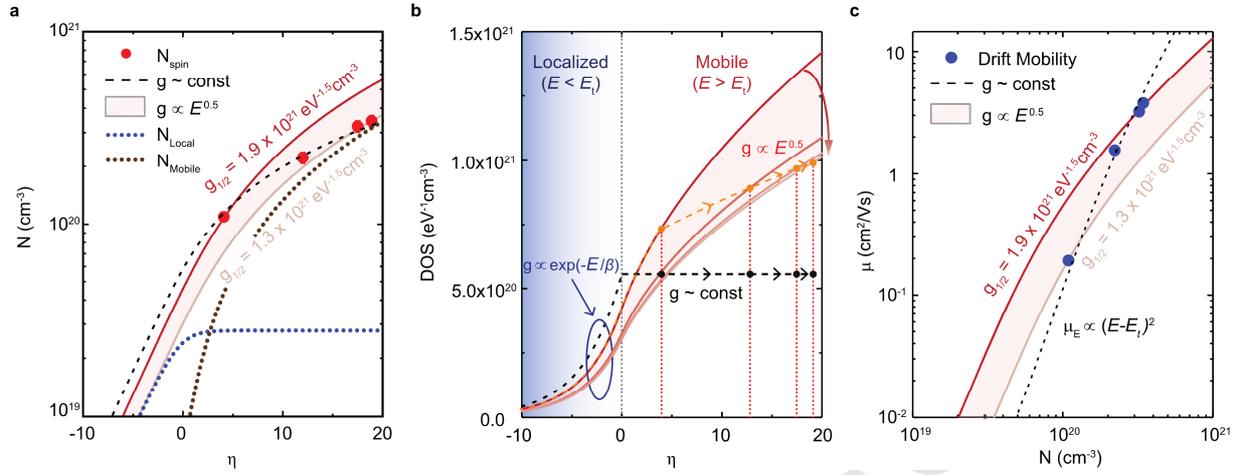
Figure 4: **Density of states calculation and mobility variation with doping.**

**a**, Charge concentration in PBTTT/F$_4$-TCNQ variation with $\eta$ experimentally determined from the number of localized spins (red circles), N$_{spin}$, counted by ESR measurements. Two different DOS models were used to fit the N versus $\eta$ data; $i = 0$ model (black-dashed line, a constant $g(E)$ at $E \geq E_t$) and $i = 1/2$ model with a range of $g_{1/2}$ (light pink area bounded by a dark red and a light red lines, $g(E)^{0.5}$ at $E \geq E_t$). The concentration of mobile and localized carriers are shown as brown dotted lines and blue dotted lines, respectively, for $i = 1/2$ and $g_{1/2} = 1.3 \times 10^{21}$ eV$^{-1.5}$cm$^{-3}$. **b**, The DOS profiles for the $i = 0$ and $i = 1/2$ models used in **a**. The blue shaded region represents the localized tail states which result in an exponential DOS profile at $E < E_t$. The orange dots and black dots represent the values of the DOS at the positions of $\eta$ at each N$_{spin}$ measured by ESR. The red block arrow (with a varying color strength) shows the evolution of the DOS profile predicted by the non-static $i = 1/2$ model as $\eta$ increases. **c**, The plot for carrier mobility, $\mu$, calculated by $\sigma/Ne$ for each N$_{spin}$ (dark blue circles). The $i = 0$ model gives the best fit for the data range which predicts $\mu_E \propto (E - E_t)^2$.
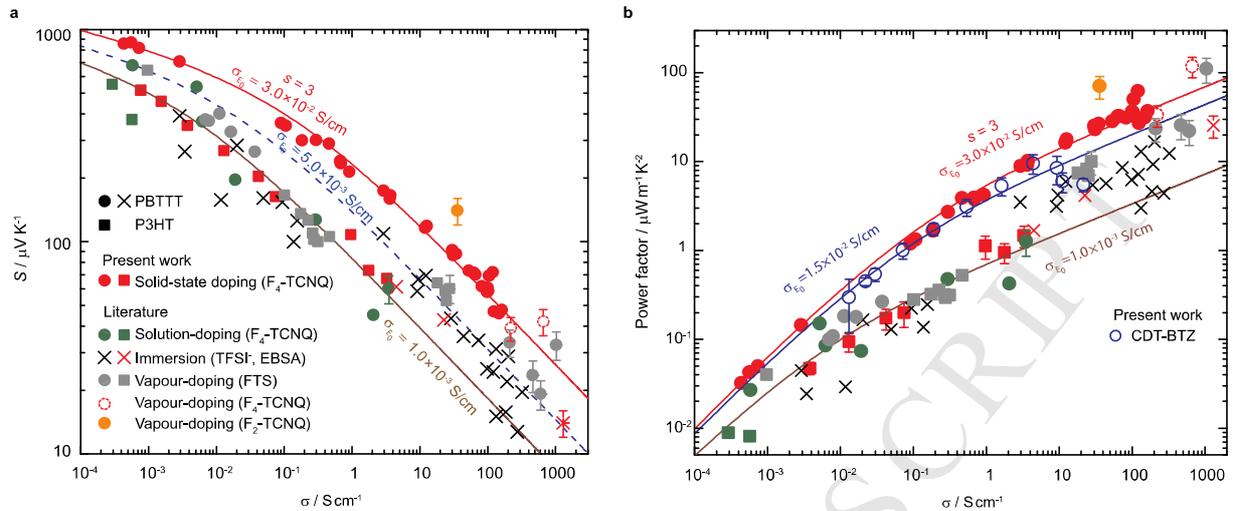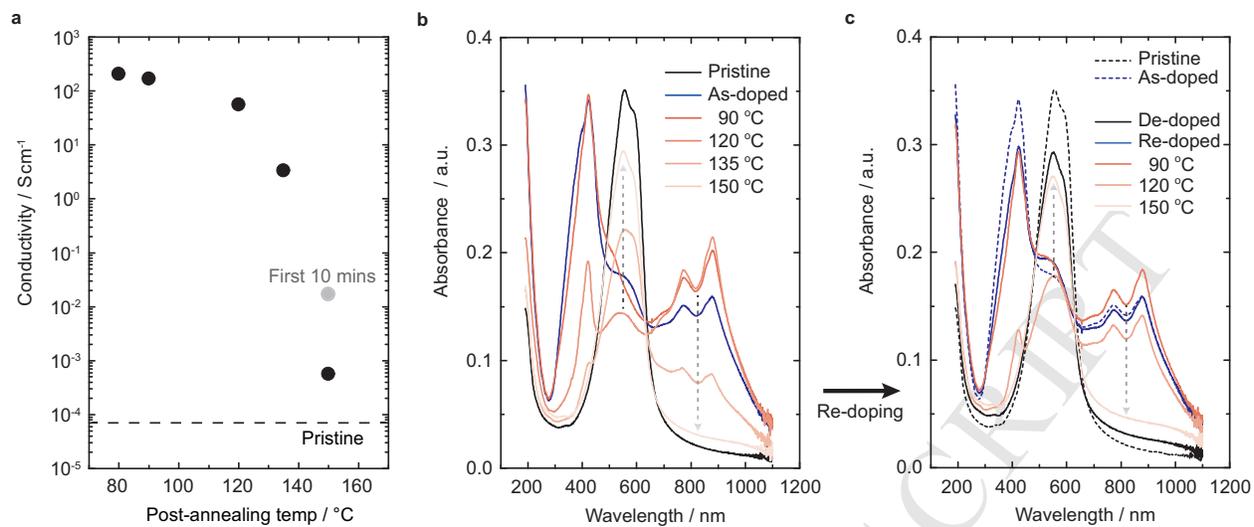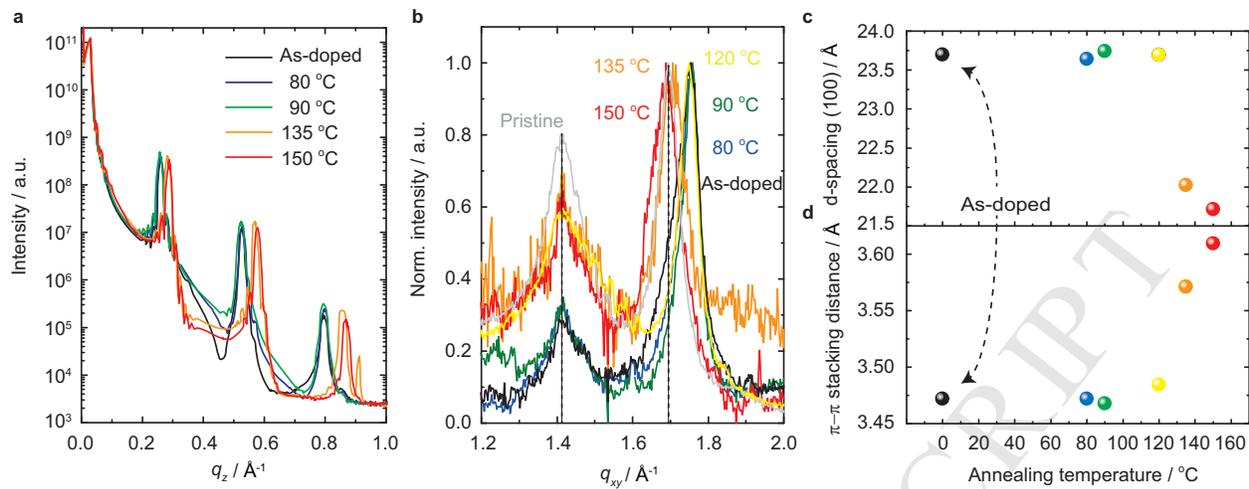
Figure 5: **Comparison of Seebeck coefficient and thermoelectric power factor variation with different doping methods. a**, Comparison of conductivity with Seebeck coefficient data reported in literature for PBTTT (solid circles and crosses) and P3HT (solid squares) with various doping methods: solution-doping with $F_4$-TCNQ [16](green), PBTTT film doped by immersion in a solution containing TFSI$^-$ [61] (black cross) and immersion in an EBSA solution [62] (red cross), FTS vapour doping (grey) [16, 62] The present work with solid-state doping of PBTTT produces the highest $\sigma_{E_0}$ compared to other doping methods. The data were taken from a compiled plot by Glaudell et al. [16] and Patel et al. [62]. **b**, Calculated power factor ($S^2\sigma$) of PBTTT (red solid circles), CDT-BTZ (blue hollow circles) and P3HT (brown solid squares) doped with $F_4$-TCNQ with the solid-state doping method from the present work, plotted together with the data from literature in **a**. The same fits for different $\sigma_{E_0}$ in **a** were translated to power factor versus conductivity plots.
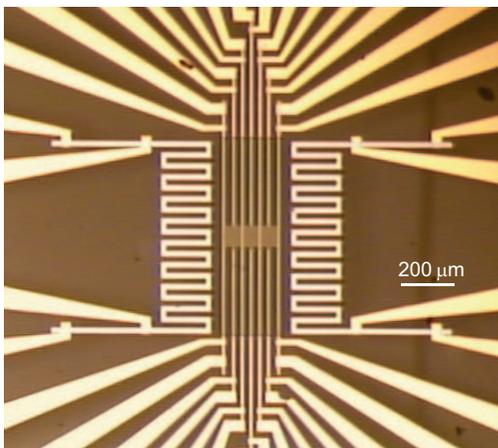
**Summary for Table of Conents**

The thermoelectric response of highly conducting polymers including poly(2,5-bis(3-tetradecylthiophen-2-yl)thieno[3,2-b]thiophene) doped by solid-state diffusion of tetrafluoro-tetracyanoquinodimethane is investigated over a wide range of doping levels by a controllable de-doping. The Seebeck coefficient-conductivity relationship reveals the underpinning strong energy dependence of charge transport and sheds light upon crucial transport parameters that enhance the thermoelectric power factor in conducting polymers.

**a**



200 μm

**b**



$s = 3$ $\sigma_{E0} =$

— 3.0×10⁻² S/cm
- - - 2.0×10⁻² S/cm
- - - 4.0×10⁻² S/cm
— 1.5×10⁻² S/cm
- - - 5.0×10⁻³ S/cm
— 1.0×10⁻³ S/cm

••••• $s = 0$ (Mobiity-edge model)

- PBTTT
- CDT-BTZ
- P3HT

$S$ / μV K⁻¹

$\sigma$ / S cm⁻¹